



## Shot noise and differential conductance as signatures of putative topological superconductivity in $\text{FeSe}_{0.45}\text{Te}_{0.55}$

Ka Ho Wong <sup>1</sup>, Eric Mascot,<sup>1</sup> Vidya Madhavan,<sup>2</sup> Dale J. Van Harlingen,<sup>2</sup> and Dirk K. Morr <sup>1</sup>

<sup>1</sup>University of Illinois at Chicago, Chicago, Illinois 60607, USA

<sup>2</sup>University of Illinois at Urbana Champaign, Champaign, Illinois 61801, USA



(Received 28 September 2021; revised 3 June 2022; accepted 3 June 2022; published 21 June 2022)

We present a theory for the differential shot noise,  $dS/dV$ , as measured via shot-noise scanning tunneling spectroscopy, and the differential conductance,  $dI/dV$ , for tunneling into Majorana zero modes (MZMs) in the putative topological superconductor  $\text{FeSe}_{0.45}\text{Te}_{0.55}$ . We demonstrate that for tunneling into chiral Majorana edge modes near domain walls, as well as MZMs localized in vortex cores and at the end of defect lines,  $dS/dV$  vanishes whenever  $dI/dV$  reaches a quantized value being equal to the quantum of conductance. These results are independent of the particular orbital tunneling path, thus establishing a vanishing  $dS/dV$  concomitant with a quantized  $dI/dV$ , as universal signatures for Majorana modes in two-dimensional topological superconductors, irrespective of the material's specific complex electronic band structure.

DOI: [10.1103/PhysRevB.105.L220504](https://doi.org/10.1103/PhysRevB.105.L220504)

**Introduction.** The unambiguous experimental identification of Majorana zero modes (MZMs) in topological superconductors, the putative building blocks for topological quantum computing, has remained a major challenge. While it has been predicted that the differential conductance,  $dI/dV$ , for tunneling into MZMs is quantized both for one-dimensional [1,2] and two-dimensional topological superconductors [3], and that the shot noise associated with the tunneling into Majorana modes exhibits various characteristic signatures [1,4–10], the experimental verification of these predictions has remained difficult due to the close proximity of trivial in-gap states, as well as small superconducting gaps. Recent experiments, however, have provided enthralling evidence for the existence of topological surface superconductivity in the iron-based superconductor  $\text{FeSe}_{0.45}\text{Te}_{0.55}$  possessing a full  $s_{\pm}$ -wave gap of a few meV. In particular, these experiments have reported the existence of a surface Dirac cone [11], of MZMs in the vortex core [12–14] and at the end of line defects [15] in monolayer  $\text{FeSe}_{0.45}\text{Te}_{0.55}$ , and of a Majorana edge mode at a domain wall [16]. While the physical origin of this putative topological phase has remained a question of debate, being ascribed either to the existence of a topological insulator whose surface Dirac cone is gapped out by proximitized superconductivity [11,17], or to the interplay [18] of an  $s_{\pm}$ -wave gap, a Rashba spin-orbit interaction, and recently observed surface ferromagnetism [19,20], the question naturally arises as to what type of universal physical observables associated with the existence of localized MZMs or chiral Majorana edge modes can be expected in the multiorbital  $\text{FeSe}_{0.45}\text{Te}_{0.55}$  compound.

The development of scanning tunneling shot-noise spectroscopy [21–25] has opened a new approach to investigating this question as it allows the direct measurement of the local shot noise associated with electron tunneling into a Majorana mode, thus complementing the measurement of the differential conductance (for a review on the experimental

implementation of shot noise measurements, see Ref. [26]). Using a Keldysh Green's function approach, we compute the differential shot noise,  $dS/dV$ , and differential conductance,  $dI/dV$ , using a recently proposed five-orbital model for  $\text{FeSe}_{0.45}\text{Te}_{0.55}$  in which the topological superconducting phase arises from the interplay of surface magnetism, a Rashba spin-orbit interaction, and a hard superconducting gap with  $s_{\pm}$  symmetry [18]. Specifically, we study  $dS/dV$  and  $dI/dV$  for three different occurrences of Majorana modes: a chiral Majorana edge mode at a domain wall, and MZMs in vortex cores and at the end of line defects. We demonstrate that for each of these cases, the electron tunneling into a Majorana mode is accompanied by a vanishing differential shot noise,  $dS/dV$ , and a quantized differential conductance,  $dI/dV$ , being equal to the quantum of conductance. Since these results hold for tunneling into each of the five relevant orbitals, they demonstrate that a quantized  $dI/dV$ , and a vanishing  $dS/dV$  are universal signatures for Majorana modes in two-dimensional topological superconductors, that are independent of the material's specific complex electronic band structure. This, in turn, allows one to employ the vanishing of the differential shot noise as a local marker to detect topological phases. Finally, we show that the measurement of a nonvanishing supercurrent along a domain wall using a scanning SQUID (superconducting quantum interference device) microscope (SSM) [27] is a third characteristic signature for the existence of Majorana modes, thus complementing those features found in  $dS/dV$  and  $dI/dV$ . The combination of our results points toward new possibilities for the experimental identification of Majorana modes in complex electronic materials.

**Theoretical model.** To investigate the shot noise and differential conductance associated with the tunneling into Majorana modes on the surface of  $\text{FeSe}_{0.45}\text{Te}_{0.55}$ , we consider a two-dimensional five-orbital model [28,29] that was obtained from a fit to angle-resolved photoemission spectroscopy

(ARPES) and scanning tunneling spectroscopy (STS) experiments [29] and was recently proposed to explain the emergence of topological superconductivity in  $\text{FeSe}_{0.45}\text{Te}_{0.55}$  as arising from the interplay between (i) a full superconducting  $s_{\pm}$ -wave gap, (ii) surface magnetism, evidence for which was recently reported by ARPES [19] and quantum sensing [20] experiments, and (iii) a Rashba spin orbit interaction that arises from the breaking of the inversion symmetry on the surface. The resulting Hamiltonian in real space is given by

$$\begin{aligned}
H_0 = & - \sum_{a,b=1}^5 \sum_{\mathbf{r},\mathbf{r}',\sigma} t_{\mathbf{r},\mathbf{r}'}^{ab} c_{\mathbf{r},a,\sigma}^\dagger c_{\mathbf{r}',b,\sigma} - \sum_{a=1}^5 \sum_{\mathbf{r},\sigma} \mu_{aa} c_{\mathbf{r},a,\sigma}^\dagger c_{\mathbf{r},a,\sigma} \\
& + i\alpha \sum_{a=1}^5 \sum_{\mathbf{r},\delta,\sigma,\sigma'} c_{\mathbf{r},a,\sigma}^\dagger (\boldsymbol{\delta} \times \boldsymbol{\sigma})_{\sigma\sigma'}^\zeta c_{\mathbf{r}+\delta,a,\sigma'} \\
& - J \sum_{a=1}^5 \sum_{\mathbf{r},\sigma,\sigma'} \mathbf{S}_{\mathbf{r}} \cdot c_{\mathbf{r},a,\sigma}^\dagger \boldsymbol{\sigma}_{\sigma\sigma'} c_{\mathbf{r},a,\sigma'} \\
& + \sum_{a=1}^5 \sum_{\langle\langle\mathbf{r},\mathbf{r}'\rangle\rangle} \Delta_{\mathbf{r}\mathbf{r}'}^{aa} c_{\mathbf{r},a,\uparrow}^\dagger c_{\mathbf{r}',a,\downarrow}^\dagger + \text{H.c.} \quad (1)
\end{aligned}$$

Here  $a, b = 1, \dots, 5$  are the orbital indices corresponding to the  $d_{xz}, d_{yz}, d_{x^2-y^2}, d_{xy}$ , and  $d_{3z^2-r^2}$  orbitals, respectively,  $-t_{\mathbf{r}\mathbf{r}'}^{ab}$  represents the electronic hopping amplitude between orbital  $a$  at site  $\mathbf{r}$  and orbital  $b$  at site  $\mathbf{r}'$  on a two-dimensional square lattice,  $\mu_{aa}$  is the on-site energy in orbital  $a$ ,  $c_{\mathbf{r},a,\sigma}^\dagger$  ( $c_{\mathbf{r},a,\sigma}$ ) creates (annihilates) an electron with spin  $\sigma$  at site  $\mathbf{r}$  in orbital  $a$ , and  $\boldsymbol{\sigma}$  is the vector of spin Pauli matrices. The superconducting order parameter  $\Delta_{\mathbf{r}\mathbf{r}'}^{aa}$  represents intraorbital pairing between next-nearest neighbor Fe sites  $\mathbf{r}$  and  $\mathbf{r}'$  (in the 1 Fe unit cell), yielding a superconducting  $s_{\pm}$ -wave symmetry [29]. Moreover,  $\alpha$  represents the Rashba spin-orbit interaction arising from the breaking of the inversion symmetry at the surface [30] with  $\boldsymbol{\delta}$  being the vector connecting nearest neighbor sites.  $\mathbf{S}_{\mathbf{r}}$  denotes the ferromagnetically ordered moment [19,20] of magnitude  $S$  which is locally exchange coupled to the conduction electrons via an interaction  $J$ . The observation of ARPES experiments [19] are consistent with a considerable fraction of the ordered magnetic moment aligned perpendicular to the surface, such that we assume an out-of-plane ferromagnetic alignment of  $\mathbf{S}_{\mathbf{r}}$  for concreteness. In the normal state, the Hamiltonian of Eq. (1) yields three Fermi surfaces in the 1-Fe Brillouin zone whose orbital character implies that the superconducting order parameter is nonzero only in the  $d_{xz}, d_{yz}$ , and  $d_{xy}$  orbitals [29]. Finally, as shown in Ref. [18], this model exhibits a series of topological phases that are characterized by the Chern number,  $C$ .

To compute the differential conductance and differential shot noise in a topological superconducting phase, we employ the Keldysh Green's function formalism [31,32]. In general, there exist five different tunneling amplitudes,  $t_a$  ( $a = 1, \dots, 5$ ), for electron tunneling between the tip and the five  $d$  orbitals in the system [33]. For simplicity, we assume for the results shown below that only one of these tunneling amplitudes is nonzero at a time. In addition, we assume that the electrons tunnel into a single site  $\mathbf{r}$  of the system, an assumption that is justified by the picometer spatial resolution of STS experiments [34]. The current flowing between the tip

and orbital  $a$  at site  $\mathbf{r}$  in the system is then given by

$$I(V) = \frac{2et_a}{h} \sum_{\sigma=\uparrow,\downarrow} \int_{-\infty}^{\infty} d\varepsilon \text{Re}[G_{ts}^<(\mathbf{r}, a, \sigma, \sigma, \varepsilon)], \quad (2)$$

with  $a = 1, \dots, 5$  being the orbital indices, and for the zero-frequency shot noise we find

$$\begin{aligned}
S(\omega = 0, V) & = \frac{2e^2 t_a^2}{h} \sum_{\sigma,\sigma'=\uparrow,\downarrow} \int_{-\infty}^{\infty} d\varepsilon [G_{tt}^>(\sigma, \sigma', \varepsilon) G_{ss}^<(\sigma', \sigma, \varepsilon) \\
& + G_{ss}^>(\sigma, \sigma', \varepsilon) G_{tt}^<(\sigma', \sigma, \varepsilon) + [F_{ss}^>(\sigma, \sigma', \varepsilon)]^* \\
& \times F_{tt}^<(\sigma', \sigma, \varepsilon) + [F_{tt}^>(\sigma, \sigma', \varepsilon)]^* F_{ss}^<(\sigma', \sigma, \varepsilon) \\
& - G_{ts}^>(\sigma, \sigma', \varepsilon) G_{ts}^<(\sigma', \sigma, \varepsilon) - G_{st}^>(\sigma, \sigma', \varepsilon) G_{st}^<(\sigma', \sigma, \varepsilon) \\
& - [F_{st}^>(\sigma, \sigma', \varepsilon)]^* F_{st}^<(\sigma', \sigma, \varepsilon) \\
& - [F_{ts}^>(\sigma, \sigma', \varepsilon)]^* F_{ts}^<(\sigma', \sigma, \varepsilon)]. \quad (3)
\end{aligned}$$

Here,  $G, F$  are the normal and anomalous Green's functions, with  $t, s$  denoting the sites of the tip and the system between which electrons tunnel, and all Green's functions involving the system are evaluated at site  $\mathbf{r}$  and for orbital  $a$  [for details, see Supplemental Material (SM) [35], Sec. I].  $dI/dV$  and  $dS/dV$  are then obtained by differentiating Eqs. (2) and (3), respectively.

*Results.* There are three distinct cases in which Majorana modes emerge from the above described theoretical model for  $\text{FeSe}_{0.45}\text{Te}_{0.55}$ : chiral Majorana edge modes along domain walls, MZMs located in vortex cores, as well as MZMs located at the end of line defects [18]. We begin by studying the form of  $dS/dV$  and  $dI/dV$  for chiral Majorana edge modes that emerge at a domain wall separating a topological  $C = 1$  region from a trivial  $C = 0$  region. The observation of strong disorder in  $\text{FeSe}_{0.45}\text{Te}_{0.55}$  [36,37], combined with the fact that MZMs are not observed in all vortex cores, suggest that such domain walls could be realized on the surface of  $\text{FeSe}_{0.45}\text{Te}_{0.55}$ . In Fig. 1(a), we present the electronic dispersion as a function of momentum along the domain wall, showing two Majorana modes traversing the superconducting gap. We note that as we consider a system with periodic boundary conditions, the system considered here contains two domain walls, with a Chern number change of  $\Delta C = 1$  at each of the domain walls, resulting in two Majorana modes, one located at each of the domain walls. In Fig. 1(b), we show a linecut of the local density of states across the domain wall: it shows an almost energy independent spectral weight inside the superconducting gap near the domain wall, arising from the chiral Majorana edge mode. In order to identify the universal features of the differential shot noise and differential conductance associated with the tunneling into a single Majorana state of this chiral edge mode, however, we need to (i) resolve the Majorana states in energy, which can be done by considering a finite length of the domain wall, leading to discretized energy levels as revealed by the LDOS shown in Figs. 1(c), and (ii) ensure that a finite lifetime of the Majorana states arises solely from its coupling to the tip. In Fig. 1(d), we present the voltage dependence of both  $dS/dV$  and  $dI/dV$  near the lowest-energy Majorana state, for tunneling into the  $d_{xy}$  orbital. Note that due to the finite size of the system we

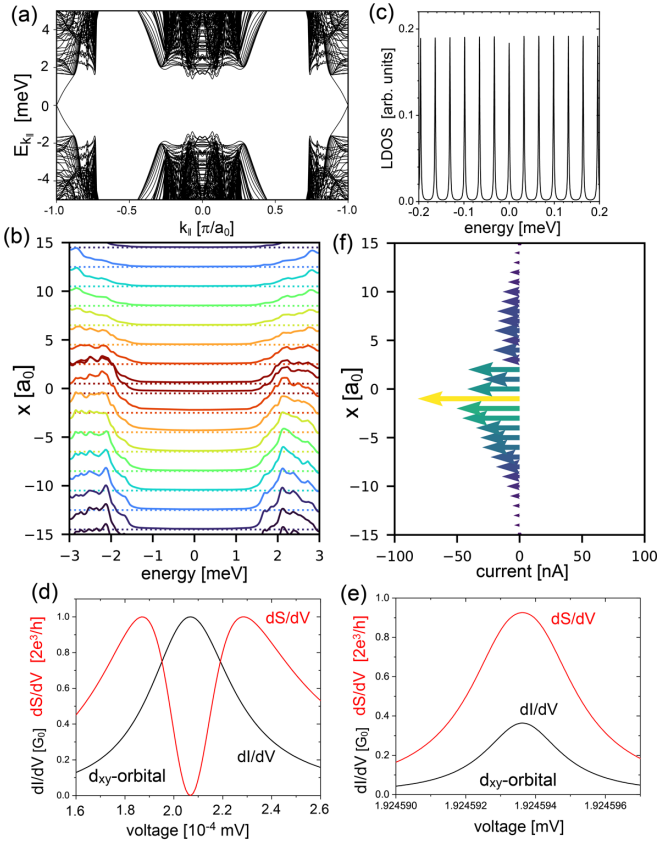


FIG. 1. Domain wall with  $\alpha = 7$  meV separating a topological  $C = 1$  region with  $JS = 7.5$  meV from a trivial  $C = 0$  region with  $J = 0$ . (a) Electronic dispersion as a function of momentum along the domain wall. The chiral Majorana edge mode traverses the superconducting gap. (b) LDOS along a linecut perpendicular to the domain wall. (c) Low-energy LDOS in which individual Majorana states are energetically resolved.  $dS/dV$  (red line) and  $dI/dV$  (black line) for (d) the lowest-energy Majorana state, and (e) for a state near the gap edge with  $E = 1.9245$  meV. (f) Spatial profile of the supercurrent near the domain wall.

consider, the lowest-energy Majorana state is located at a very small, but finite energy. As previously reported, we find that  $dI/dV$  reaches the quantum of conductance,  $G_0$ , at the energy of the Majorana state [3], implying that at this energy, the transmission amplitude reaches unity. A qualitatively new feature of the Majorana modes is revealed by the differential shot noise,  $dS/dV$ , which vanishes at that bias where  $dI/dV$  reaches  $G_0$ . Defining a transmission amplitude  $T(V)$  via  $dI/dV = G_0 T(V)$ , we find that the differential shot noise obeys  $dS/dV \sim T(V)[1 - T(V)]$  (see SM, Sec. II). This is similar to the previously established relation between the current  $I$  and noise  $S$  [38], and accounts for the discrete nature of the MZM. The same result holds for tunneling into any of the other  $d$  orbitals that possess spectral weight at the domain wall (see SM, Sec. II), implying that a quantized conductance and vanishing differential shot noise are universal features that are independent of the complex multiorbital structure of a topological superconductor. We note, however, that the width of the  $dI/dV$  and  $dS/dV$  curves, which arises from the coupling between the orbitals and the tip, varies between the orbitals,

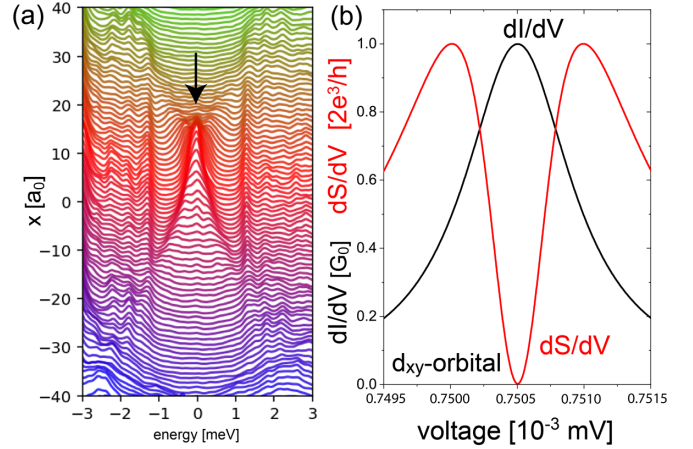


FIG. 2. (a) Linecut of the LDOS through the center of a vortex core in the topological  $C = 1$  phase with  $(\alpha, JS) = (7, 8)$  meV for a uniform magnetic flux of 1 Wb, revealing the existence of a MZM. (b)  $dI/dV$  (black line) and  $dS/dV$  (red line) for tunneling into the MZM for the  $d_{xy}$  orbital.

as follows from a comparison of the results shown in Fig. 1(d) with those for the  $d_{xz}$  orbital in Fig. S1(a) (see SM, Sec. II). This is a direct consequence of the different spectral weight of the Majorana mode in the five  $d$  orbitals, which is accounted for in our calculations as we compute the Green's functions in Eqs. (2) and (3) both in real and orbital space. Thus, our results reveal orbital-dependent effects both in  $dI/dV$  and  $dS/dV$ .

Moreover, a quantized  $dI/dV$  and vanishing  $dS/dV$  are also found for higher-energy Majorana states, until one approaches states near the gap edge. Indeed, for states close to the gap edge, we find significant deviations of  $dI/dV$  from  $G_0$ , while  $dS/dV$  does not vanish any longer, as shown in Fig. 1(e). This demonstrates that both a quantized value for  $dI/dV$  and the vanishing of  $dS/dV$  are hallmarks of chiral Majorana edge modes. Concomitant with these results, we find that the domain wall carrying a chiral Majorana edge mode also gives rise to a nonvanishing supercurrent that flows parallel to the domain wall, as shown in Fig. 1(f). In contrast, as previously shown [18], domain walls that possess only trivial low-energy states do not exhibit a net supercurrent along the domain wall. Since such supercurrents can be detected using an SSM scanned along the domain wall [27], the combination of  $dI/dV$ ,  $dS/dV$ , and SSM measurements can provide strong evidence for the existence of Majorana modes along a domain wall.

We next study the differential shot noise associated with the tunneling into a localized MZM in a vortex core by implementing the magnetic field via the Peierls substitution and compute the spatial dependence of the superconducting order parameters in the  $d_{xz}$ ,  $d_{yz}$ , and  $d_{xy}$  orbitals self-consistently (for details, see Ref. [18]). In Fig. 2(a) we plot a linecut of the LDOS through the center of the vortex core in the  $C = 1$  phase, which reveals the existence of a MZM in its center (see black arrow). In Fig. 2(b), we present  $dS/dV$  and  $dI/dV$ , associated with the tunneling into this localized MZM. As expected, we again find that at the bias when  $dI/dV$  reaches the quantized quantum of conductance,  $dS/dV$  vanishes. As shown in SM, Sec. III, this result holds for tunneling into

any of the  $d$  orbitals, again supporting our conclusion that these results are universal and independent of any complex electronic band structure.

Finally, we consider the emergence of zero-energy states at the end of line defects, recently observed in monolayer  $\text{FeSe}_{0.5}\text{Te}_{0.5}$  deposited on a  $\text{SrTiO}_3$  substrate [15], whose spatial structure is similar to that expected for MZMs. It is presently unclear whether these MZMs are a characteristic feature of an underlying topological phase as argued in Ref. [18], similar to line defect MZMs predicted to occur in topological ( $p_x + ip_y$ )-wave superconductors [39], or are independent of it, simply utilizing the monolayer's complex electronic structure to form a one-dimensional topological superconductor as proposed in Refs. [15,40,41]. Indeed, it is presently unknown whether the  $\text{FeSe}_{0.5}\text{Te}_{0.5}/\text{SrTiO}_3$  system itself is topological or not. While the mechanism proposed in Refs. [11,17] requires a three-dimensional bulk structure, and thus would not apply to this system, the mechanism described by Eq. (1) could give rise to topological superconductivity if  $\text{FeSe}_{0.5}\text{Te}_{0.5}/\text{SrTiO}_3$  were also to exhibit ferromagnetism (which is presently unknown). Here, we follow the argumentation of Ref. [18], which has demonstrated that the emergence of MZMs at the end of line defects is a characteristic feature of the underlying topological phase. To study  $dS/dV$  and  $dI/dV$  associated with these line defect MZMs, we represent the line defect for simplicity as a line of potential scatterers (though magnetic scatterers could also be realized [40,41]) described by the Hamiltonian

$$H_{def} = U_0 \sum_{a=1}^5 \sum_{\mathbf{R}, \sigma} c_{\mathbf{R}, a, \sigma}^\dagger c_{\mathbf{R}, a, \sigma}, \quad (4)$$

where  $U_0$  is the potential scattering strength, and the sum runs over all sites  $\mathbf{R}$  of the line defect. As previously shown [18], when the underlying system is in a topological phase, there exist certain ranges of the scattering potential  $U_0$  in which localized zero-energy states emerge at the end of the line defect, whose spatial LDOS structure is consistent with that of MZMs, as shown in Fig. 3(a). In contrast, the next higher-energy state is delocalized along the chain, as shown in Fig. 3(b). This qualitative difference between these two states is also reflected in the form of  $dI/dV$  and  $dS/dV$ . For tunneling into the lowest-energy state, we again find that when  $dI/dV$  reaches  $G_0$ ,  $dS/dV$  vanishes, as shown in Fig. 3(c), establishing that this state is a MZM. This result holds for tunneling into all of the five Fe  $d$  orbitals (see SM, Sec. IV). In contrast, for the next higher-energy state [see Fig. 3(d)],  $dI/dV$  does not reach  $G_0$ , and  $dS/dV$  does not vanish, implying that this state is not topological in nature. Since  $dS/dV$  vanishes at the energy of a Majorana mode, a measurement of  $dS/dV$  can be employed to identify topological phases. For example, consider the evolution of the lowest-energy state,  $E_0$ , associated with the line defect as a function of the scattering strength  $U_0$  shown in Fig. 3(e). For those regions of  $U_0$  with  $E_0 = 0$  (shown with a gray background), we find that the differential shot noise for tunneling into the  $d_{yz}$  and  $d_{x^2-y^2}$  orbitals also vanishes. In contrast, already for small deviations of  $E_0$  from zero, on the order of 1% of the superconducting gap size,  $dS/dV$  exhibits significant deviations from zero, indicating that the lowest-energy state is no longer topolog-

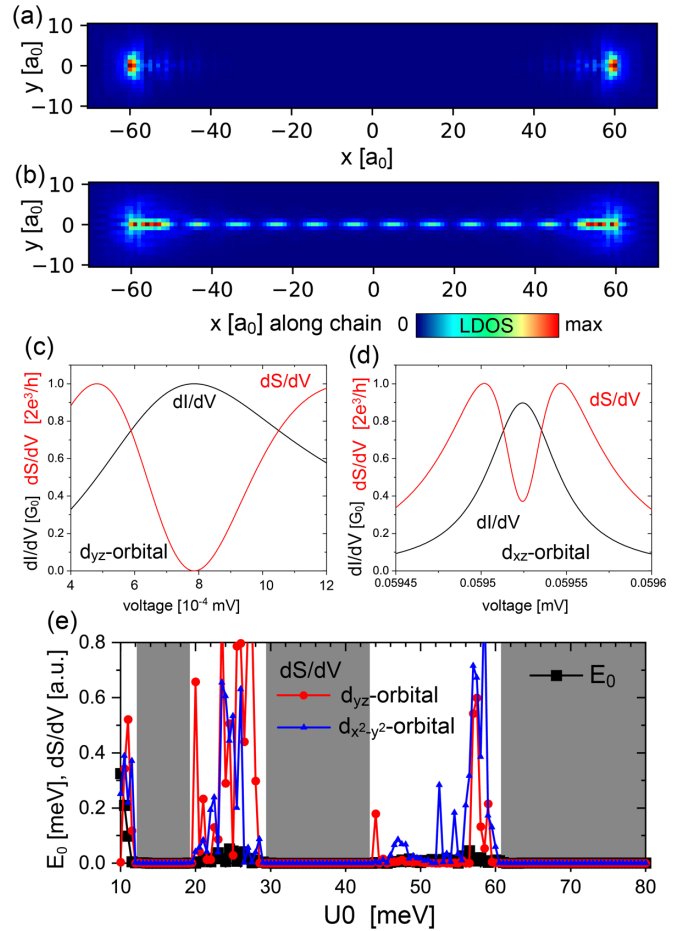


FIG. 3. Spatial structure of the LDOS around a line defect with  $(\alpha, JS) = (7, 7.5)$  meV for (a) the lowest-energy state at  $E_0 = 0.000786$  meV, and (b) the next higher-energy state at  $E_1 = 0.0595$  meV. The line defect has a length  $L = 120a_0$  with scattering strength  $U = 72.5$  meV. (c), (d) The respective  $dI/dV$  (black line) and  $dS/dV$  (red line) for tunneling into the  $d_{xy}$  orbital near energies corresponding to panels (a) and (b), respectively. (e) The energy of the lowest-energy state, as well as  $dS/dV$  for tunneling into the  $d_{xy}$  and  $d_{x^2-y^2}$  orbitals, as a function of  $U_0$ .

ical. Moreover, to further elucidate the differences between MZMs and trivial (near) zero-energy states, we compare in SM, Sec. V the spatially resolved transport signatures of a line defect MZM with those of a trivial Yu-Shiba-Rusinov state [42–44] induced by a magnetic impurity; the latter can be tuned to zero energy by adjusting the magnetic scattering potential. In addition to the examples discussed above, this comparison again shows that the transport signatures of MZMs and trivial (near) zero-energy states are qualitatively different, implying that  $dS/dV$  and  $dI/dV$  represent a sensitive probe for the topological nature of (near) zero-energy states.

Finally, we want to briefly discuss the effects of disorder and finite temperature on the results presented above. To consider the former, we added some disorder in the form of additional potential scattering sites to the end of the line defect shown in Fig. 3 (see SM, Sec. VI for details). This disorder neither affects the existence of the MZM (in agreement with earlier results [3]), nor changes the quantization of  $dI/dV$  or

the vanishing of  $dS/dV$  for tunneling into the MZM. We thus conclude that our results are robust against disorder effects, as long as the disorder is not strong enough to destroy the topological phase [45]. Moreover, while a nonzero temperature leads to a deviation of  $dI/dV$  and  $dS/dV$  from their  $T = 0$  results, we find that these deviations are strongly suppressed (see SM, Sec. VI) as long as  $k_B T$  is smaller than the energy width of the MZM induced by its coupling to the STM tip, in qualitative agreement with earlier results for  $dI/dV$  [46]. Thus, by moving the STM tip closer to the surface, and hence increasing the tunneling amplitude, thermal broadening effects can be reduced. The unique form of  $dI/dV$  and  $dS/dV$  related to an MZM are of course lost once  $k_B T$  is sufficiently large to excite trivial higher-energy states.

*Conclusions.* In conclusion, we have studied the form of the differential noise,  $dS/dV$ , and the differential conductance,  $dI/dV$ , for tunneling into localized MZMs in vortex cores and at the end of line defects, and into chiral Majorana edge modes in  $\text{FeSe}_{0.45}\text{Te}_{0.55}$ . Using a five-band model that was previously extracted from fits to ARPES and STS experiments [29], we demonstrated that for all three cases, when the differential conductance  $dI/dV$  reaches the quantum of conductance, the differential shot noise,  $dS/dV$ , as measured via scanning tunneling shot noise spectroscopy, vanishes. In contrast, for low-energy states that are trivial,  $dS/dV$  remains finite. These results demonstrate that  $dS/dV$  is a sensitive probe for the topological nature of low-energy states, being able to discriminate between topological and

trivial low-energy states. This ability, in turn, can be employed to detect topological phase transitions. These results hold for tunneling into any of the Fe  $d$  orbitals of  $\text{FeSe}_{0.45}\text{Te}_{0.55}$ , demonstrating that they are independent of the material's specific complex electronic band structure. In addition, we showed that a nonzero net supercurrent flows along domain walls separating topological and trivial regions, in contrast to domain walls that possess only trivial low-energy states, as previously shown [18]. Thus, the combination of differential shot noise, differential conductance, and measurements of local supercurrents via scanning probe microscopy techniques can provide a unique fingerprint for the existence of topological Majorana modes.

*Acknowledgments.* We would like to thank S. Rachel for stimulating discussions. The theoretical work on supercurrents and the differential conductance near domain walls was supported by the U.S. Department of Energy, Office of Science, Basic Energy Sciences, under Award No. DE-FG02-05ER46225 (E.M. and D.K.M.). The theoretical work on the differential shot noise was supported by the Center for Quantum Sensing and Quantum Materials, an Energy Frontier Research Center funded by the U.S. Department of Energy, Office of Science, Basic Energy Sciences under Award No. DE-SC0021238 (K.H.W. and D.K.M.). V.M. and D.J.V.H. acknowledge support by the Center for Quantum Sensing and Quantum Materials, an Energy Frontier Research Center funded by the U.S. Department of Energy, Office of Science, Basic Energy Sciences under Award DE-SC0021238.

- 
- [1] K. T. Law, P. A. Lee, and T. K. Ng, Majorana Fermion Induced Resonant Andreev Reflection, *Phys. Rev. Lett.* **103**, 237001 (2009).
- [2] K. Flensberg, Tunneling characteristics of a chain of Majorana bound states, *Phys. Rev. B* **82**, 180516(R) (2010).
- [3] S. Rachel, E. Mascot, S. Cocklin, M. Vojta, and D. K. Morr, Quantized charge transport in chiral Majorana edge modes, *Phys. Rev. B* **96**, 205131 (2017).
- [4] C. J. Bolech and E. Demler, Observing Majorana Bound States in  $p$ -Wave Superconductors Using Noise Measurements in Tunneling Experiments, *Phys. Rev. Lett.* **98**, 237002 (2007).
- [5] B. Zocher and B. Rosenow, Modulation of Majorana-Induced Current Cross-Correlations by Quantum Dots, *Phys. Rev. Lett.* **111**, 036802 (2013).
- [6] M. Diez, I. C. Fulga, D. I. Pikulin, J. Tworzydło, and C. W. J. Beenakker, Bimodal conductance distribution of Kitaev edge modes in topological superconductors, *New J. Phys.* **16**, 063049 (2014).
- [7] D. E. Liu, M. Cheng, and R. M. Lutchyn, Probing Majorana physics in quantum-dot shot-noise experiments, *Phys. Rev. B* **91**, 081405(R) (2015).
- [8] T. Jonckheere, J. Rech, A. Zazunov, R. Egger, A. L. Yeyati, and T. Martin, Giant Shot Noise from Majorana Zero Modes in Topological Trijunctions, *Phys. Rev. Lett.* **122**, 097003 (2019).
- [9] C. W. J. Beenakker and D. O. Oriekhov, Shot noise distinguishes Majorana fermions from vortices injected in the edge mode of a chiral  $p$ -wave superconductor, *SciPost Phys.* **9**, 080 (2020).
- [10] V. Perrin, M. Civelli, and P. Simon, Discriminating Majorana bound states by tunneling shot-noise tomography, *Phys. Rev. B* **104**, L121406 (2021).
- [11] P. Zhang, K. Yaji, T. Hashimoto, Y. Ota, T. Kondo, K. Okazaki, Z. Wang, J. Wen, G. D. Gu, H. Ding, and S. Shin, Observation of topological superconductivity on the surface of an iron-based superconductor, *Science* **360**, 182 (2018).
- [12] D. Wang, L. Kong, P. Fan, H. Chen, S. Zhu, W. Liu, L. Cao, Y. Sun, S. Du, J. Schneeloch, R. Zhong, G. Gu, L. Fu, H. Ding, and H.-J. Gao, Evidence for Majorana bound states in an iron-based superconductor, *Science* **362**, 333 (2018).
- [13] T. Machida, Y. Sun, S. Pyon, S. Takeda, Y. Kohsaka, T. Hanaguri, T. Sasagawa, and T. Tamegai, Zero-energy vortex bound state in the superconducting topological surface state of  $\text{Fe}(\text{Se},\text{Te})$ , *Nat. Mater.* **18**, 811 (2019).
- [14] S. Zhu, L. Kong, L. Cao, H. Chen, M. Papaj, S. Du, Y. Xing, W. Liu, D. Wang, C. Shen, F. Yang, J. Schneeloch, R. Zhong, G. Gu, L. Fu, Y.-Y. Zhang, H. Ding, and H.-J. Gao, Nearly quantized conductance plateau of vortex zero mode in an iron-based superconductor, *Science* **367**, 189 (2020).
- [15] C. Chen, K. Jiang, Y. Zhang, C. Liu, Y. Liu, Z. Wang, and J. Wang, Atomic line defects and zero-energy end states in monolayer  $\text{Fe}(\text{Te},\text{Se})$  high-temperature superconductors, *Nat. Phys.* **16**, 536 (2020).
- [16] Z. Wang, J. O. Rodriguez, L. Jiao, S. Howard, M. Graham, G. D. Gu, T. L. Hughes, D. K. Morr, and V. Madhavan, Evidence for dispersing 1D Majorana channels in an iron-based superconductor, *Science* **367**, 104 (2020).

- [17] Z. Wang, P. Zhang, G. Xu, L. K. Zeng, H. Miao, X. Xu, T. Qian, H. Weng, P. Richard, A. V. Fedorov, H. Ding, X. Dai, and Z. Fang, Topological nature of the  $\text{FeSe}_{0.5}\text{Te}_{0.5}$  superconductor, *Phys. Rev. B* **92**, 115119 (2015).
- [18] E. Mascot, S. Cocklin, M. Graham, M. Mashkooi, S. Rachel, and D. K. Morr, Topological surface superconductivity in  $\text{FeSe}_{0.45}\text{Te}_{0.55}$ , [arXiv:2102.05116](https://arxiv.org/abs/2102.05116) [Commun. Phys. (to be published)].
- [19] N. Zaki, G. Gu, A. Tsvetlik, C. Wu, and P. D. Johnson, Time-reversal symmetry breaking in the Fe-chalcogenide superconductors, *Proc. Natl. Acad. Sci. USA* **118**, e2007241118 (2021).
- [20] N. J. McLaughlin, H. Wang, M. Huang, E. Lee-Wong, L. Hu, H. Lu, G. Q. Yan, G. Gu, C. Wu, Y.-Z. You, and C. R. Du, Strong correlation between superconductivity and ferromagnetism in an Fe-chalcogenide superconductor, *Nano Lett.* **21**, 7277 (2021).
- [21] H. Birk, M. J. M. de Jong, and C. Schönenberger, Shot-Noise Suppression in the Single-Electron Tunneling Regime, *Phys. Rev. Lett.* **75**, 1610 (1995).
- [22] U. Kemiktarak, T. Ndukum, K. C. Schwab, and K. L. Ekinci, Radio-frequency scanning tunnelling microscopy, *Nature (London)* **450**, 85 (2007).
- [23] M. Herz, S. Bouvron, E. Cavar, M. Fonin, W. Belzig, and E. Scheer, Fundamental quantum noise mapping with tunnelling microscopes tested at surface structures of subatomic lateral size, *Nanoscale* **5**, 9978 (2013).
- [24] K. M. Bastiaans, D. Cho, T. Benschop, I. Battisti, Y. Huang, M. S. Golden, Q. Dong, Y. Jin, J. Zaanen, and M. P. Allan, Charge trapping and super-Poissonian noise centres in a cuprate superconductor, *Nat. Phys.* **14**, 1183 (2018).
- [25] F. Masee, Y. K. Huang, M. S. Golden, and M. Aprili, Noisy defects in the high- $T_c$  superconductor  $\text{Bi}_2\text{Sr}_2\text{CaCu}_2\text{O}_{8+x}$ , *Nat. Commun.* **10**, 544 (2019).
- [26] F. Masee, Q. Dong, A. Cavanna, Y. Jin, and M. Aprili, Atomic scale shot-noise using cryogenic MHz circuitry, *Rev. Sci. Instrum.* **89**, 093708 (2018).
- [27] E. M. Spanton, K. C. Nowack, L. Du, G. Sullivan, R.-R. Du, and K. A. Moler, Images of Edge Current in InAs/GaSb Quantum Wells, *Phys. Rev. Lett.* **113**, 026804 (2014).
- [28] S. Graser, T. A. Maier, P. J. Hirschfeld, and D. J. Scalapino, Near-degeneracy of several pairing channels in multiorbital models for the Fe pnictides, *New J. Phys.* **11**, 025016 (2009).
- [29] S. Sarkar, J. Van Dyke, P. O. Sprau, F. Masee, U. Welp, W.-K. Kwok, J. C. Seamus Davis, and D. K. Morr, Orbital superconductivity, defects, and pinned nematic fluctuations in the doped iron chalcogenide  $\text{FeSe}_{0.45}\text{Te}_{0.55}$ , *Phys. Rev. B* **96**, 060504(R) (2017).
- [30] S. Nadj-Perge, I. K. Drozdov, J. Li, H. Chen, S. Jeon, J. Seo, A. H. MacDonald, B. A. Bernevig, and A. Yazdani, Observation of Majorana fermions in ferromagnetic atomic chains on a superconductor, *Science* **346**, 602 (2014).
- [31] L. V. Keldysh, Diagram technique for nonequilibrium processes, *J. Exp. Theor. Phys.* **20**, 1018 (1965).
- [32] C. Caroli, R. Combescot, P. Nozieres, and D. Saint-James, Direct calculation of the tunneling current, *J. Phys. C: Solid State Phys.* **4**, 916 (1971).
- [33] J. M. Blanco, F. Flores, and R. Pérez, STM-theory: Image potential, chemistry and surface relaxation, *Prog. Surf. Sci.* **81**, 403 (2006).
- [34] M. H. Hamidian, I. A. Firmo, K. Fujita, S. Mukhopadhyay, J. W. Orenstein, H. Eisaki, S. Uchida, M. J. Lawler, E.-A. Kim, and J. C. Davis, Picometer registration of zinc impurity states in  $\text{Bi}_2\text{Sr}_2\text{CaCu}_2\text{O}_{8+\delta}$  for phase determination in intra-unit-cell Fourier transform STM, *New J. Phys.* **14**, 053017 (2012).
- [35] See Supplemental Material at <http://link.aps.org/supplemental/10.1103/PhysRevB.105.L220504> for further support for the conclusions and results presented in the main text.
- [36] D. Cho, K. M. Bastiaans, D. Chatzopoulos, G. D. Gu, and M. P. Allan, A strongly inhomogeneous superfluid in an iron-based superconductor, *Nature (London)* **571**, 541 (2019).
- [37] D. Wang, R. Zhong, G. Gu, and R. Wiesendanger, Surface orbital order and chemical potential inhomogeneity of the iron-based superconductor  $\text{FeTe}_{0.55}\text{Se}_{0.45}$  investigated with special STM tips, *Phys. Rev. Research* **3**, L032055 (2021).
- [38] M. Büttiker, Scattering Theory of Thermal and Excess Noise in Open Conductors, *Phys. Rev. Lett.* **65**, 2901 (1990).
- [39] M. Wimmer, A. R. Akhmerov, M. V. Medvedyeva, J. Tworzydło, and C. W. J. Beenakker, Majorana Bound States without Vortices in Topological Superconductors with Electrostatic Defects, *Phys. Rev. Lett.* **105**, 046803 (2010).
- [40] Y. Zhang, K. Jiang, F. Zhang, J. Wang, and Z. Wang, Atomic Line Defects and Topological Superconductivity in Unconventional Superconductors, *Phys. Rev. X* **11**, 011041 (2021).
- [41] X. Wu, J.-X. Yin, C.-X. Liu, and J. Hu, Topological magnetic line defects in Fe(Te,Se) high-temperature superconductors, [arXiv:2004.05848](https://arxiv.org/abs/2004.05848).
- [42] L. Yu, Bound state in superconductors with paramagnetic impurities, *Acta Phys. Sin.* **21**, 75 (1965).
- [43] H. Shiba, Classical spins in superconductors, *Prog. Theor. Phys.* **40**, 435 (1968).
- [44] A. I. Rusinov, On the theory of gapless superconductivity in alloys containing paramagnetic impurities, *J. Exp. Theor. Phys.* **29**, 1101 (1969).
- [45] E. Mascot, C. Agrahar, S. Rachel, and D. K. Morr, Stability of disordered topological superconducting phases in magnet-superconductor hybrid systems, *Phys. Rev. B* **100**, 235102 (2019).
- [46] G.-H. Feng and H.-H. Zhang, Probing robust Majorana signatures by crossed Andreev reflection with a quantum dot, *Phys. Rev. B* **105**, 035148 (2022).